Research Article

PGME Alkaline Wastewater Distillate Treatment by an Alkaliphilic Microbial Consortium: Optimization using Response Surface Methodology with Central Composite Design (RSM-CCD)

Lance Angelo Tamondong Rovillos
School of Graduate Studies, School of Chemical, Biological, and Materials Engineering and Sciences, Mapúa University, Manila, Philippines

Khyle Glainmer Nagtalon Quiton and Kristopher Ray Simbulan Pamintuan*
School of Chemical, Biological, and Materials Engineering and Sciences, School of Graduate Studies, Mapúa University, Manila, Philippines

Siang Chen Wu
Environmental Molecular Microbiology Laboratory, Department of Environmental Engineering, National Chung Hsing University, Taichung, Taiwan

* Corresponding author. E-mail: krspamintuan@mapua.edu.ph DOI: 10.14416/j.asep.2026.06.003
Received: 16 October 2025; Revised: 20 November 2025; Accepted: 17 March 2026; Published online: 4 June 2026

Abstract
Glycol ethers, especially propylene glycol methyl ether, are widely used as organic solvents in many fields. Although physicochemical treatments are relatively common in treating industrial effluents, their production produces wastewater with extreme conditions like high alkalinity and high chemical oxygen demand (COD), warranting the need for alternatives. In this study, response surface methodology (RSM) was adapted to optimize the operating conditions for the treatment of propylene glycol methyl ether-alkaline wastewater distillate (PGME-AWD) using an alkaliphilic microbial consortium. Thirteen reactors were run according to a central composite design (CCD), creating surface models for peak percentage COD removal, COD removal rate constant, and percentage true color (TC) change by changing values for the factors: initial reactor pH (IRP) from 7.0 to 11.0 and initial substrate concentration (ISC) from 1.0 %v/v to 3.0 %v/v. Pseudo-first order kinetics, with the highest average regression coefficient (RSQ) value from curve-fitting, was used to calculate rate constant parameters. Numerical integration was used to obtain TC parameters. Based on the models obtained, optimal conditions for the responses include the following: IRP of 8.569 and ISC of 1.038 %v/v for the first; IRP of 8.566 and ISC of 1.00 %v/v for the second; and 11.000 and ISC of 3.000 %v/v for the third. This shows that optimizing the third response contradicts the optimization of the first two responses, suggesting separation of treatment into stages: one for COD removal and one for color and turbidity.

Keywords: Central composite design, Chemical oxygen demand removal, Kinetics, Optimization, Response surface methodology, True color change

1 Introduction

The development of human technologies, although paving the way for advancement and addressing additional requirements for human consumption, had, and is continuously resulted in an increased volume of waste effluents that contain a number of toxic compounds, which in many cases, cannot be degraded using conventional treatment methods. On a global scale, about 42% of the total volume of wastewater can be attributed to various industrial processes [1].

On a relevant note, chemical characterization and source attribution reveal a wide variation of pollutants present in wastewater across different industries, with one study revealing about 227 ± 128 different organic compounds across just 22 different enterprises in China [2]. This entails that a treatment procedure for the collected wastewater of one type of industry may not be sufficient nor applicable for another, and properly recognizing this issue is necessary in the development of efficient wastewater treatment strategies.

Furthermore, while many industrial sectors produce wastewater containing conventional pollutants, the semiconductor industry comes off as particularly concerning because of toxic and persistent wastewater, much of which is proprietary and thus, characterization is usually constrained [3]. Wastewater properties from this, however, still vary from process to process and also depend on pre–treatment methods done, which result in pH changes ranging from acidic to alkaline [4]. Glycol ethers, for instance, are widely used as organic solvents in processes with an oil-water interface. They are being used as general solvents in the printed circuit board (PCB) industry and as photoresist material in the production of semiconductor chips [5]. One of the safer alternatives in the glycol ether groups of compounds, propylene glycol methyl ether (PGME), is manufactured mostly in the more selective base–catalyzed reactions [6], [7]. As such, wastewater produced from these processes is extremely alkaline. Moreover, the industry is posing a threat to water usage and safety as its global requirement within the market continues to rise, as forecasted by the World Semiconductor Trade Statistics [8].

Biological wastewater treatment methods have seen an increase in applications in recent years [9], [10], [11]. They mainly operate on the fact that microorganisms can handle organic wastes and convert them into simpler forms [12]. Although physicochemical treatments are better established than biological methods, extreme conditions warrant a need for process adaptation as these often lead to higher rates of fouling, decreased efficiency, and higher resistance because of increased formation of precipitates [13], [14]. Unlike these methods, extremophiles can function well in extreme environments. Among these are those that can live in alkaline conditions, known as alkaliphilic bacteria [15]. Given the problems encountered by existing treatment methods in terms of long–term efficiency and costs under conditions of high pH and chemical oxygen demand (COD), biological treatment using alkaliphilic microbes presents an ideal and sustainable approach. Moreover, tackling this opportunity promotes two Sustainable Development Goals (SDGs): responsible consumption and production (SDG 12) by directly contributing to meeting targets 12.4 and 12.9; and clean water and sanitation (SDG 6) through target 6.3 [16].

As a statistical optimization tool, response surface methodology (RSM) explores the possibility of interplay between each independent factor in modelling the response, aside from effectively lowering costs and operational time [17]. By employing a central composite design (CCD), this method is already being used in a number of studies concerning biological wastewater treatment methods [10], [18]–[20]. Ultimately, however, there is a scarcity of resources discussing the treatment of wastewater specifically generated from the production of PGME, even more so on the use of an alkaliphilic microbial consortium and the optimization of operating parameters using statistical tools.

This study uniquely integrates RSM–CCD to optimize the operating conditions on the treatment of alkaline wastewater distillate (AWD), produced from the manufacture of PGME, using a consortium of alkaliphilic microbes obtained from Dongshi in Chiayi, Taiwan. Specifically, it aims to observe the effects of initial reactor pH and initial substrate concentration on the treatment performance in terms of peak percentage COD removal, COD removal rate constant, and true color (TC) change through wavelength absorbance.

2 Materials and Methods

2.1 *Bacterial consortium and alkaline wastewater distillate*

The bacterial consortium was isolated from soil samples obtained from the rural township of Dongshi in Chiayi County, Taiwan. The pH of the soil was determined to have a slight alkalinity, measuring 7.8. The consortium was then cultured and enriched in a sequential batch reactor whose pH and COD levels were monitored continuously through regular sampling. Since microbial consortia from soils are oligotrophic in nature, culture medium was formulated to simulate their natural environment [21], [22]. However, in this study, AWD is added as the carbon

source in the medium along with the formulated micronutrient and macronutrient solutions. Medium replacement was done by draining the reactor halfway, and a version of the medium, twice concentrated, is fed semi-batch every cycle. This causes the initial pH of the medium to be around 11.5 to 12.0, causing the reactor to be alkaline at around 9.0 to 9.5 after feeding.

The AWD was sourced from a company within the chemical manufacturing industry in the vicinity of Taiwan. This company manufactures propylene glycol methyl ether, and its wastewaters are extremely alkaline with a pH of 13.9 and highly polluted with a measured COD concentration of about 26,500 mg/L. With the nutrient solutions, it served as substrate for the batch experiments.

2.2 *Reactor media, inoculation, and setup*

Similar to the culture medium, the media for the reactors were formulated by accounting for the consortium's oligotrophic nature. Growth media for the batch reactors were prepared using a 10× diluted nutrient solution whose concentrated formulations are shown in Table 1 [21], [22]. In lieu of the carbon sources used in previous cultures, the growth media contained these nutrient solutions and AWD at different loading rates as formulated using a CCD matrix. Deionized water was used to make up for the volume balance.

Table 1: Formulations of macronutrient and micronutrient solutions.

10× Concentrated Macronutrient Solution (g/L)		100× Concentrated Micronutrient Solution (g/L)	
$CaSO_4 \cdot 2H_2O$	0.6	$MnSO_4 \cdot H_2O$	0.22
$MgSO_4 \cdot 7H_2O$	1.0	$ZnSO_4 \cdot 7H_2O$	0.05
NaCl	0.8	H_3BO_3	0.05
KNO_3	1.03	$CuSO_4 \cdot 5H_2O$	0.0025
$NaNO_3$	6.89	$Na_2MoO_4 \cdot 2H_2O$	0.0025
Na_2HPO_4	1.11	$CoCl_2 \cdot 6H_2O$	0.0046

After the reactor media were set up, inoculation was done. To minimize block errors, all inocula were isolated at the same time from the enrichment culture as a single volume of 75 mL. This was then centrifuged at 17,000 rpm at a temperature of 25 degrees Celsius. The pellets were washed and resuspended using a less concentrated variation of the medium and without the AWD, and then a vortex machine was used to homogenize the mixture. All inocula were then obtained from this mixture. In this study, each of the batch reactors was inoculated with 10 %v/v using the isolated consortium from the culture. The reactors were then kept in an orbital shaker set at 120 rpm and at a temperature of 30 °C and samples were taken once every day.

2.3 *Optimizing variables and design of experiments*

This study involved the investigation of initial reactor pH (IRP) and initial substrate concentration (ISC) as factors for optimizing three response variables.

2.3.1 Initial reactor pH

The first factor considered in this study is the IRP (may be referred to as F1 or Factor 1). Although alkaliphilic extremophiles are known to have optimized growth in the pH range of 9.0–10.0 [15], for this study, response measurements were done for a wider range of 7.0–11.0. Coupled with the CCD layout for the variables, this enabled the researcher to observe the consortium's behavior from slightly acidic to extremely basic pH values. Since the AWD had a pH of around 13.9, 1.0 M sulfuric acid (H_2SO_4) was added dropwise for pH amendment.

2.3.2 Initial substrate concentration

Along with IRP, the ISC (may be referred to as F2 or Factor 2) was also investigated as an optimizing variable. COD removal and TC change were measured, and the COD removal rate constants were determined under different AWD loading rates. Since the AWD had elevated COD values as it is, dilution with the base culture medium was necessary to provide different organic loading values and ensure that it remains the limiting factor in the reactor. In this study, values for the ISC were based on trial runs, which showed consortium activity in the 1.0–3.0 %v/v range.

2.3.3 Experimental design

This study used Response Surface Methodology (RSM), carried out using Design Expert v13, for the design of the experiments, mathematical modelling, and graphical representations of results with the goal of optimizing the three response variables, peak percentage COD removal, COD removal rate constant, and true color change, using the two independent factors, IRP and ISC.

The five–level full factorial Central Composite Design (CCD) was chosen and implemented for the study, reducing the number of trials from a typical one–factor–at–a–time design, exploring possible interplays between factors and enabling investigation of responses just outside the set range of the independent factors through its alpha levels. The range and levels for the operating variables are presented in Table 2. A total of thirteen runs were conducted to accommodate various interaction models for optimization.

Table 2: Levels of independent variables for CCD.

Factor	$-\alpha$	−1	0	+1	$+\alpha$
Initial Reactor pH	6.17	7.0	9.0	11.0	11.83
Initial Substrate Concentration, %v/v	0.59	1.0	2.0	3.0	3.41

2.4 *Variables for optimization*

This study involved the investigation of the performance of conditions set by the design of experiments in terms of peak percentage COD removal, COD removal rate constant, and wavelength absorbance and true color change.

2.4.1 Peak percentage COD removal

Chemical oxygen demand for each reactor was measured daily from the start up to the end of the batch experimentations. CODs were calculated from the measurements obtained using a Hitachi U2900 double beam spectrophotometer. Prior to measurement, samples collected were digested for 2 hours using potassium dichromate ($K_2Cr_2O_7$) with silver sulfate ($AgSO_4$) as a catalyst. COD levels were determined from a calibration curve prepared from diluted aliquots of a standard COD solution made from potassium hydrogen phthalate. The peak percentage COD removal (may be referred to as R1 or Response 1 from this point onwards) for a reactor was calculated using Equation (1), where $\%\ COD_{removed}$ is the percent COD removal, COD_0 is the initial COD level, and COD_t is the COD level after treatment time t [17], [19], [23].

$$\%\ COD_{removed} = \frac{COD_0 - COD_t}{COD_0} \times 100\% \quad (1)$$

2.4.2 COD removal rate constant

Aside from the actual removal of COD, kinetics, in the form of a rate constant (may be referred to as R2 or Response 2 from this point onwards), is an integral and objective point of comparison between the batch experiments. Although the mechanisms for the substrate removal can be hard to describe numerically and depend on numerous factors, kinetic models are often used to parametrize these reaction mechanisms and comparisons are made using these parameters.

In this study, removal kinetics were explained using pseudo–zeroth order (M0), pseudo–first order (M1), pseudo–second order (M2), and sigmoidal function models, namely, the logistic (ML), Gompertz (MG), and Richards (MR) models, which were modified to fit growth curves. Fitting was done through MATLAB R2024b using the lsqcurvefit function for uniformity.

2.4.3 Wavelength absorbance and true color change

TC change (referred to as R3 or Response 3 from this point onwards) for each reactor was measured daily from the start up to the end of the batch experimentations to gauge a possible relationship between true color and COD levels. True colors were quantified through numerical integration of the absorbance measurements obtained across the wavelength range of 480 nm – 510 nm using a Hitachi U2900 double beam spectrophotometer.

This range was decided based on the performance of different wavelength ranges in predicting the dilution extent of the original wastewater, which was done through linear regression of measured absorbance values of solutions of known dilution. The Simpson's 3/8 rule for numerical integration can be expanded when the number of data points can be given by four added to a multiple of three. This results in a composite form of the rule, which was able to be applied to the absorbance, as shown in Equation (2), where $f(x)$ is the absorbance at the wavelength x and n is the number of uniform segments from which the width is defined [24], [25].

$$\int_{x_0}^{x_n} f(x)dx \approx \frac{3}{8}\left(\frac{x_n - x_0}{n}\right)\begin{pmatrix} f(x_0) + 3\sum_{i=1,\,4,\,7,\,\ldots}^{n-2} f(x_i) + \\ 3\sum_{i=2,\,5,\,8,\,\ldots}^{n-1} f(x_i) + \\ 2\sum_{i=3,\,6,\,9,\,\ldots}^{n-3} f(x_i) + f(x_n) \end{pmatrix} \quad (2)$$

3 Results

Table 3 shows the actual setup of variables for each run and the summary of results obtained through measurement and calculations in the optimization study with factors, initial reactor pH and initial substrate concentration. Thirteen runs with varying IRP from 6.17 to 11.83 and ISC from 0.59 %v/v to 3.41 %v/v were conducted to satisfy the requirements of the design.

Table 3: Summary of actual setup of variables and results.

Run	F1	F2 (%v/v)	R1 (%)	R2 ($\times 10^{-3} h^{-1}$)	R3 (%)
1	9.0	0.59	57.2	6.2	10.5
2	9.0	2.0	52.5	4.4	6.5
3	9.0	3.41	29.3	2.3	11.9
4	11.0	3.0	18.9	1.9	27.0
5	7.0	3.0	53.6	5.9	6.3
6	11.83	2.0	0	0	30.8
7	6.17	2.0	51.5	4.6	11.4
8	9.0	2.0	52.5	4.5	9.0
9	9.0	2.0	49.0	4.0	13.0
10	9.0	2.0	45.5	3.4	4.6
11	7.0	1.0	52.1	4.4	4.8
12	11.0	1.0	29.6	2.4	18.7
13	9.0	2.0	49.0	4.1	7.9

There are different trends that can be observed from the table. Run 6 is of particular interest because of its highest TC change, even with a peak percentage COD removal of 0%. It should be noted, however, that it is the run with the highest extremum pH level of 11.83, which may have created unfavorable living conditions for the consortium, thus explains the COD removal, but may have forced reactions in the components of the medium such as formation of precipitates which are then filtered out, explaining the high TC change, since pH is a crucial factor in determining solubilities. However, a complete analysis in the form of a solubility study of the compounds present in the wastewater and medium is necessary to confirm their effects.

A similar explanation can be stated for run 4, which, when compared to run 5, had a lower IRP but the same ISC, yet obtained a higher TC change despite having a lower peak percentage of COD removal. The same goes for run 12 when compared to run 11. Regardless, these observations should not be interpreted solely as they are because ISC is a factor that was considered along with IRP when the three response variables were measured, thus proving the need for further analysis and ultimately, an optimization study.

3.1 *Peak percentage COD removal*

The dataset obtained for the COD removal from each of the 13 reactors is shown in Figure 1(a). The addition of the wastewater at five different loading capacities was evident in the initial COD levels measured. However, since the reactors were run on different IRP levels dictated by the design of the study, it can be observed that the reactors proceeded at varying rates and effectiveness expressed in percentage COD removed and calculated using Equation (1), even for those that started at the same ISC levels.

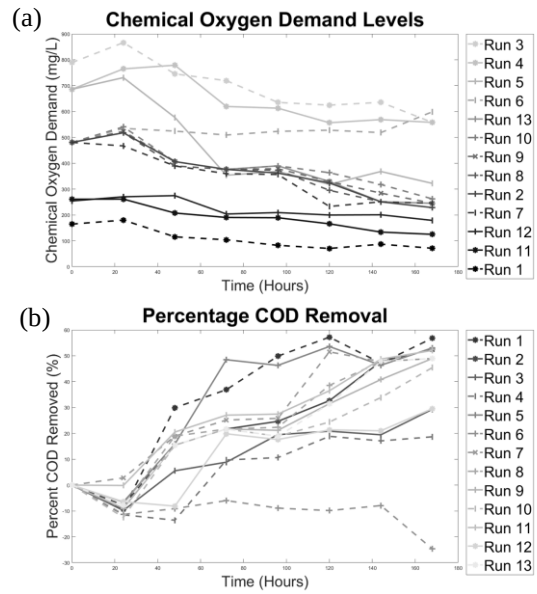

Figure 1: Actual COD levels (a) and percentage COD removal (b).

Since the reactors started at different COD loads, effectiveness is more suitably measured in percent. Reactor 1, with an IRP of 9.0 and an ISC of 0.59 %v/v, achieved the highest peak percentage COD removal of around 57.2% (Figure 1(b)). Meanwhile, reactor 6, with an IRP of 11.8 and ISC of 2 %v/v, achieved the lowest peak percentage COD removal, with as little as none from its peak COD level.

When grouped according to ISC, the effect of IRP can be observed. It is worth noting that the reactors with the lower IRP of 7.0, though not necessarily acidic, resulted to higher peak percentage

COD removal as shown in Figure 2(a). These results are comparable when thermo-alkaliphilic and halo–alkaliphilic microbial consortia were evaluated for their potential in azo–dye biodegradation and decolorization and detoxification, respectively, where efficiencies are increased in the 8 to 9 pH range and biodegradation performance were significantly lower in acidic and extremely alkali conditions [23], [26]. Furthermore, previous decolorization studies using different bacterial consortia proved to have optimum biodegradation activity in the same pH range [27], [28].

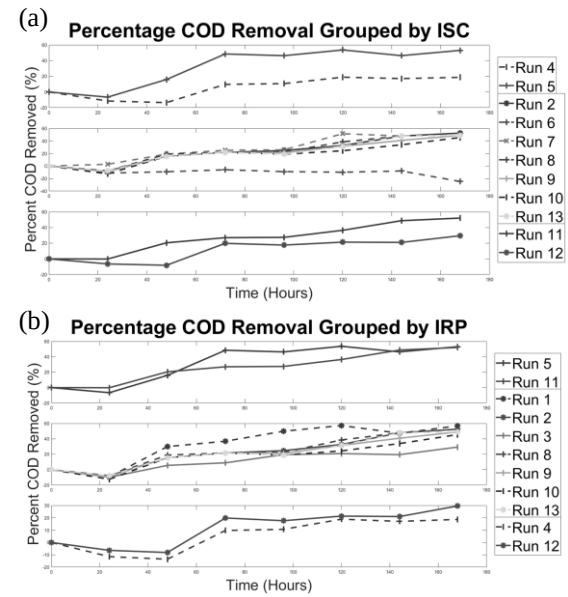

Figure 2: Percentage COD removal grouped according to ISC (a) and IRP (b).

Conversely, when grouped according to IRP, the effect of ISC can be observed. These are shown in Figure 2(b) Overall, the ISC is inversely proportional to the performance of the consortium. As in previous decolorization studies, dye biodegradation performances were also decreased as the substrate concentrations were increased [26]–[30]. This can be attributed to the potential inhibitory [31] and toxicity effects of the substrate on the consortium, as in the case of biodegradation of organic dyes [26], [28].

3.2 *Wavelength absorbance and true color change*

True color calculations were done by first measuring the absorbance of the samples within the wavelength range of 480–510 nm, then using Simpson's 3/8 rule for numerical integration, shown in Equation (2). This gave a comparable parameter in units of true color for each of the 13 reactors, which is summarized in Figure 3(a) Absorbance measurements at the start and end of the experiments are plotted in Figure 4(a) and (b).

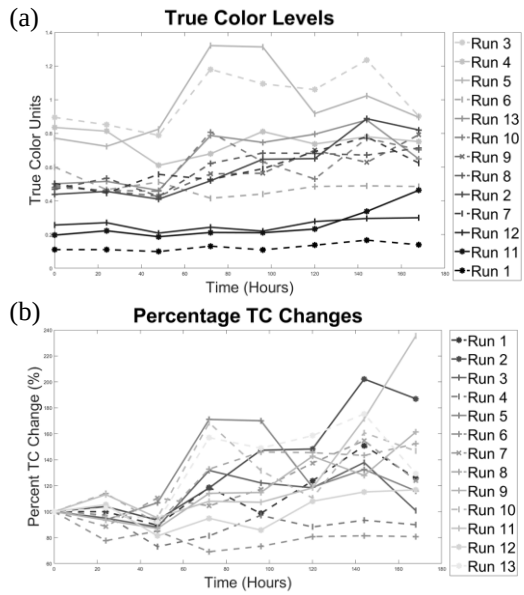

Figure 3: Absolute TC levels (a) and percentage TC change (b).

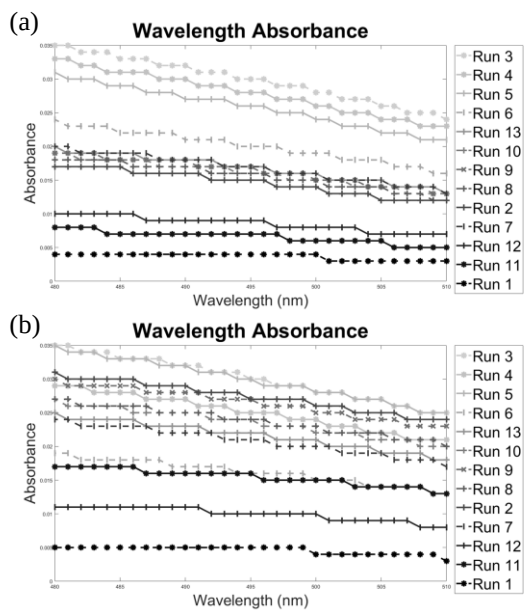

Figure 4: Wavelength absorbance for the reactors at D0 (a) and D7 (b).

Similar to the COD level measurements, the addition of the wastewater at five different loading capacities was evident in how the initial TCs are grouped. However, as it is the case for COD levels, differences in behavior can be observed even for reactors that started at the same ISCs since the reactors were run on different IRP levels.

The effectiveness of each reactor in terms of percent true color change is shown more suitably in Figure 3(b). Reactor 6, with an IRP of 11.8 and ISC of 2 %v/v, achieved the highest peak TC change of around 30.8%. On the other hand, reactor 10, with an IRP of 9.0 and ISC of 2 %v/v, achieved the lowest peak TC change of around 4.6%. These results are surprisingly different from the percent COD removal, which contributes to the significance of an optimization study. It is important to note, however, that peak TC changes occurred much earlier than peak COD removal, suggesting possible significance of optimizing for reaction time [32].

Grouping the reactors with the same ISC led to an observation on the individual effect of IRP. Unlike in COD removal, higher TC changes occurred in higher pH levels (Figure 5(a)). This is different from the results obtained when the effects of pH on both simulated and actual wastewater treatment through coagulation using acidic bio–sorbents were investigated, where acidic pH positively affected the stability of the suspension and dye adsorption [33], [34]. However, characterization analysis, which supports their findings, revealed that the physical properties of the materials work well in acidic conditions. On the other hand, alkaliphiles are known to work well on basic pH levels. In one study working with a slightly alkaline seed sludge, decolorization occurred at a much higher pH of up to 9.0 [32], [35]–[38]. Albeit, proper characterization analysis should be done to support this theory.

Grouping the reactors with the same IRP to observe the effects of ISC, a different observation from that obtained for percent COD removal can be made. Overall, the ISC is directly proportional to TC change. These are shown in Figure 5(b) In another study, direct proportionality was also observed [39]. It is important to note, however, that in most systems, the trend only holds until the optimum value, just before inhibition dominates afterwards [40], [41]. Although it may seem logical that we increase the substrate loading to further optimize TC changes, COD removal occurring at low substrate concentrations should also be of particular concern. Moreover, color absorption alone cannot describe biodegradation efficiency since metabolites and degraded fragments of the original substrate are also capable of absorbing light [42]. This only highlights the importance of an optimization study.

(a)

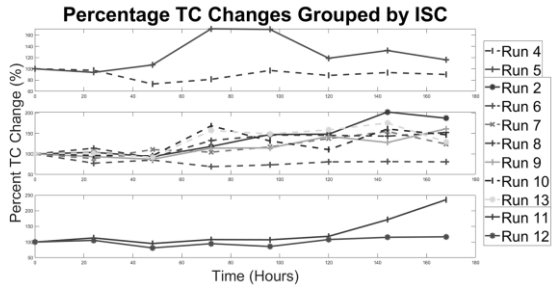

(b)

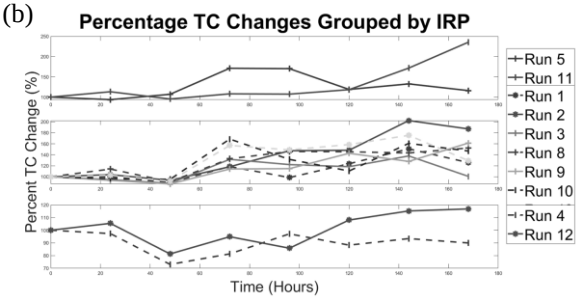

Figure 5: Percentage TC change grouped according to ISC (a) and IRP (b).

In essence, however, the individual effect of a factor cannot be fully isolated because optimization experiments are generally structured to show the effect of a variable in conjunction with other factors. A trend, however, is generally helpful as it establishes a baseline of comparison for full–factorial studies, establishment of similar and mixed systems, and validation of perturbation plots. A summary for comparison is shown in Table 4.

Table 4: Summary of optimum results and trends.

System	Comparing Factor	Optimum Results/Trend	Ref
COD Removal			
Neutral–optimized consortia	pH	7.0	[27]
Alkaline–and halo–alkaline–tolerant consortia	pH	8.0–9.0	[23], [26], [28], [31]
Specialized biological consortia	substrate concentration (treated substance)	indirectly proportional	[23], [26], [27], [28], [29], [31]

Table 4: (Continued)

System	Comparing Factor	Optimum Results/Trend	Ref
Conventional sequential biological reactor	substrate concentration (treated substance)	indirectly proportional	[30]
True Color			
Immobilized moderate systems	pH	7.0–9.0	[37], [38]
Immobilized thermophilic cyanobacterial systems	pH	8.5	[36]
Suspended systems	pH	7.0–9.0	[32], [35], [38]
Monoculture batch systems	substrate concentration (treated substance)	directly proportional initially	[39]
Microbial batch systems	substrate concentration (treated substance)	indirectly proportional	[40], [41]

4 Discussion

Further analysis of COD removal data was done to obtain the rate constants through kinetic studies. These, together with peak percentage COD removal and true color change, were then further treated with statistical tools, such as ANOVA and residual tests for assessing model qualities.

4.1 *Kinetic studies*

Table 5 is the summary of the model equations, where: C_A is the concentration at any time, t; A is the peak COD concentration; k is the rate constant for the non–sigmoidal models; μ_m is the maximum removal rate constant for the sigmoidal models; λ is the time lag for sigmoidal models; and ν is the shape factor for the modified Richards model. These are growth curves that are reparametrized to give parameters with practical biological significance [43].

To obtain a comparable rate parameter between each of the reactors, the COD removal data were fitted to the kinetic models shown above. Since reactor 6 had virtually insignificant COD removal, it was omitted from the analysis and interpretation of fit correspondence.

Each of the models' coefficient of determination (RSQ) and adjusted coefficient of determination (adjusted RSQ) was compared. Specifically, the models with the highest RSQ values were analyzed in terms of their adjusted RSQ values to account for the number of predictors and minimize the risk of overfitting. Table 6 below shows the summary of the fit for the models.

Table 5: Summary of kinetic model equations.

Model	Defining Equation	
Non–Sigmoidal Models		
Pseudo–zeroth	$C_A = A - k \cdot t$	(3)
Pseudo–first	$C_A = e^{\ln A - k \cdot t}$	(4)
Pseudo–second	$C_A = \frac{1}{\frac{1}{A} + k \cdot t}$	(5)
Sigmoidal Models		
Modified Gompertz	$C_A = A - A \cdot e^{-e^{\left[\frac{\mu_m \cdot e}{A}(\lambda - t) + 1\right]}}$	(6)
Modified Logistic	$C_A = A - \frac{A}{1 + e^{\left[\frac{4\mu_m}{A}(\lambda - t) + 2\right]}}$	(7)
Modified Richards	$C_A = A - A\left\{1 + \nu \cdot e^{[1+\nu]} \cdot e^{\left[\frac{\mu_m}{A}(1+\nu)\left(1+\frac{1}{\nu}\right)\right.}\right.$	(8)

Table 6: Summary of model fits.

Model	Average RSQ	Parameters	Average Adjusted RSQ
Non–Sigmoidal Models			
Pseudo-zeroth	0.853	A, k	0.794
Pseudo-first	0.856	A, k	0.798
Pseudo-second	0.838	A, k	0.773
Sigmoidal Models			
Modified Logistic	0.835	A, μ_m, λ	0.711
Modified Gompertz	0.850	A, μ_m, λ	0.738
Modified Richards	0.835	A, μ_m, λ, ν	0.615

As observed, although all models have an average RSQ within the range of 0.83 – 0.86, the sigmoidal models have lower average adjusted RSQ values compared to the non–sigmoidal models. This is because the former contained more predictor variables than the latter and these additional parameters did not contribute enough significance to justify their inclusion as a fitting parameter for this dataset, thus resulting in lower adjusted RSQ values.

Taking the shape factor, ν, for example, when the modified logistic model is compared to the modified Richards model. Based on the obtained individual RSQ values, shown in Table 7, and the values of the parameters obtained using the lsqcurvefit function, the modified Richards model can be simplified as the

modified logistic model when the shape factor, ν, is approximately equal to 1 [43].

Table 7: RSQ and adjusted RSQ values (in bold) for kinetic models.

Run	M0	M1	M2	ML	MG	MR
1	0.787	0.845	0.848	0.734	0.782	0.734
	0.702	**0.783**	**0.787**	**0.534**	**0.618**	**0.379**
2	0.936	0.916	0.879	0.934	0.939	0.934
	0.911	**0.883**	**0.830**	**0.885**	**0.894**	**0.847**
3	0.854	0.852	0.844	0.840	0.848	0.840
	0.796	**0.793**	**0.781**	**0.719**	**0.734**	**0.626**
4	0.681	0.675	0.663	0.680	0.689	0.680
	0.553	**0.545**	**0.528**	**0.439**	**0.456**	**0.254**
5	0.761	0.820	0.827	0.703	0.752	0.703
	0.666	**0.748**	**0.758**	**0.480**	**0.567**	**0.306**
7	0.911	0.921	0.903	0.884	0.905	0.884
	0.702	**0.889**	**0.864**	**0.797**	**0.833**	**0.729**
8	0.921	0.906	0.871	0.916	0.923	0.916
	0.911	**0.868**	**0.819**	**0.852**	**0.865**	**0.803**
9	0.917	0.903	0.874	0.909	0.916	0.910
	0.796	**0.864**	**0.824**	**0.841**	**0.853**	**0.790**
10	0.845	0.836	0.816	0.837	0.841	0.837
	0.553	**0.770**	**0.743**	**0.714**	**0.722**	**0.619**
11	0.953	0.952	0.931	0.929	0.942	0.930
	0.666	**0.933**	**0.904**	**0.876**	**0.899**	**0.837**
12	0.756	0.753	0.743	0.743	0.753	0.743
	0.702	**0.655**	**0.640**	**0.551**	**0.567**	**0.401**
13	0.908	0.888	0.854	0.910	0.913	0.910
	0.911	**0.843**	**0.795**	**0.842**	**0.847**	**0.789**

Sigmoidal models are not significantly worse, however, such as in runs 2, 8, 9, and 13, and in terms of RSQ in general. In fact, on average, the modified Gompertz model is better than the pseudo–second order model. But generally, using the dataset from this experiment, non–sigmoidal models are already sufficient to describe the reaction kinetics. Specifically, rate parameters from the pseudo–first order model will be used for the optimization study. The kinetics model for each reactor is shown in Figure 6.

4.1.1 COD removal rate constant

As it was stated in the previous response variables, differences in behavior can be observed even for reactors that started at the same ISCs since the reactors were run on different IRP levels. The characteristic of each reactor in terms of the rate constant is shown more suitably (Figure 7). Reactor 1, with an IRP of 9.0 and ISC of 0.59 %v/v, achieved the highest rate constant of around 0.0062. On the other hand, reactor 6, with an IRP of 11.8 and ISC of 2 %v/v, achieved the lowest rate constant, which was basically negligible. As expected from the results of COD removal effectiveness, the resulting rates are predictably similar.

Grouping the reactors with the same ISC led to a hypothesis on the individual effect of IRP. In general, lower IRP levels resulted in higher rate constants. These are shown in Figure 8(a). Moreover, since the reactors are arranged in increasing ISC along the x–axis, it can be observed that the bar plots peaked both

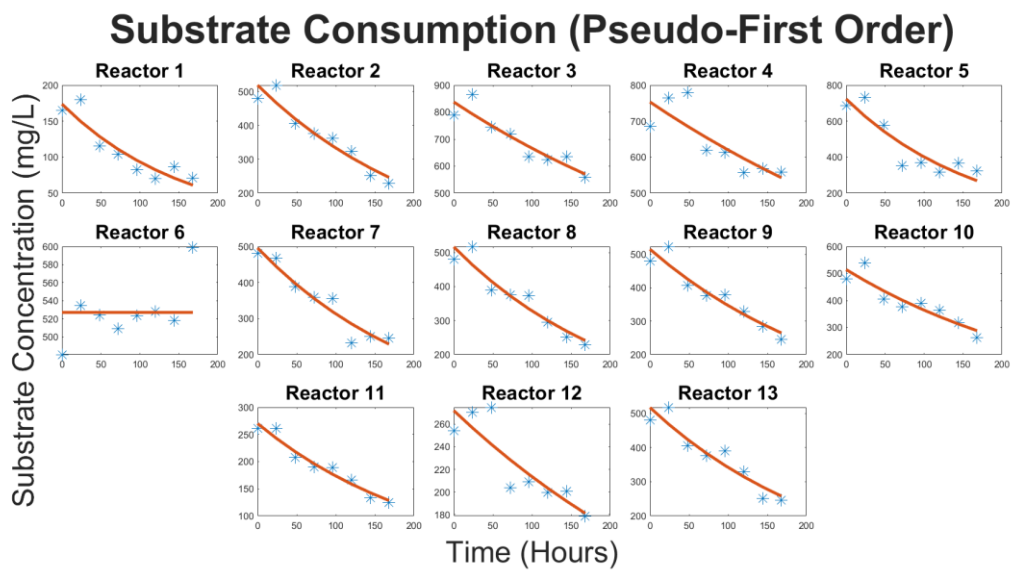

Figure 6: Substrate consumption modelled by pseudo–first order kinetics.

on the low and high ISC levels. This means that COD removal around both of these ISC regions is faster, and the design space can be shifted towards them, although their interactive behavior with IRP should also be considered. This result can be attributed to the reactor conditions at which the inoculum was cultured, but it requires further investigation. In one study that focused on the removal rates of pharmaceuticals in biofilm reactors, short–term stimulations revealed lower reaction rates for higher wastewater concentrations, but long–term adaptations showed promise in increasing the reactors' capacity to handle higher loading rates [44], [45].

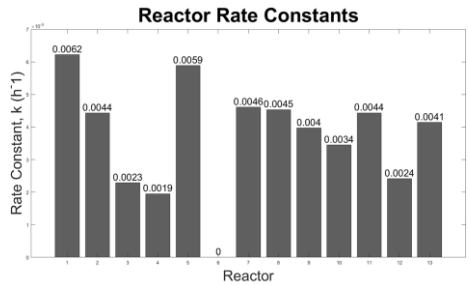

Figure 7: Calculated reactor rate constants from pseudo–first order kinetics.

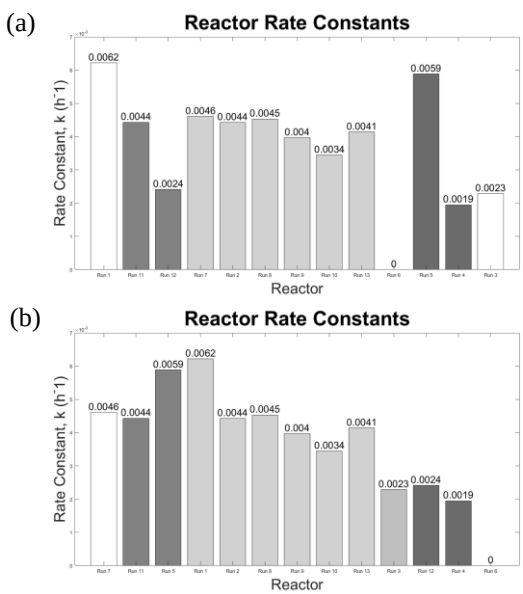

Figure 8: COD removal rate constants grouped according to ISC (a) and IRP (b).

Grouping the reactors with the same IRP, the individual effect of ISC can be observed and hypothesized. Aside from the −1 IRP level, lower ISC corresponded to higher rate constants. These are shown in Figure 8(b) Additionally, since the reactors are arranged in increasing pH along the x–axis, it can be observed that the bar plots peaked around the conditions of reactors 5 and 1, whose IRP were 7.0 and 9.0, respectively. This means that COD removal takes place faster in lower pH in the slightly basic regions of 7.0 to 9.0. For comparison, the pH of the soil from which the original consortium was sourced is 7.8 and the enrichment culture from which the inoculum was obtained is around 9.0–9.5. The design space can be tweaked and centered around this, although its interactive effects with ISC should also be considered.

4.2 *Model fitting for optimization*

The first response, peak percentage COD removal, was obtained as the maxima (peaks) of the percentage COD removal shown in Figure 1(b) The second response, the COD removal rate constant, was calculated using the pseudo–first order model for kinetics shown in Figure 7. The third response, TC change, was obtained as the absolute values of the minima (troughs) of the percentage TC change shown in Figure 3(b).

4.2.1 ANOVA on models for response variables

Models for the response variables were chosen considering maximizing fit statistics while maintaining a hierarchical structure. Reduced cubic models were fitted for peak percentage COD removal and COD removal rate constant and a reduced quadratic model for TC change.

ANOVA tests revealed that the models exhibited p–values of < 0.0001, < 0.0001, and 0.0002, noting a residual lack of fit that is of no significance as shown in Table 8. RSQ values are further discussed in the summary of fit statistics.

Table 8: Summary of ANOVA table.

Source	F–value	P–value	Remark
Peak Percentage COD Removal (Reduced Cubic)			
Model	35.80	< 0.0001	**sig.**
F1	112.33	< 0.0001	sig.
F2	20.69	0.0026	sig.
F1F2	1.98	0.2024	not sig.
$F1^2$	42.85	0.0003	sig.
$F1^2F2$	6.08	0.0431	sig.
Residual			
Lack of Fit	3.79	0.1155	**not sig.**

Table 8: (Continued)

Source	F–value	P–value	Remark
COD Removal Rate Constant (Reduced Cubic)			
Model	36.17	< 0.0001	**sig.**
F1	106.62	< 0.0001	sig.
F2	41.48	0.0004	sig.
F1F2	5.45	0.0522	
$F1^2$	25.93	0.0014	sig.
$F1^2F2$	28.94	0.0010	sig.
Residual			
Lack of Fit	0.9545	0.4950	**not sig.**
True Color Change (Reduced Quadratic)			
Model	21.94	0.0002	**sig.**
F1	56.25	< 0.0001	sig.
F2	2.03	0.1922	sig.
F1F2	1.35	0.2785	not sig.
$F1^2$	28.13	0.0007	sig.
Residual			
Lack of Fit	0.7268	0.6177	**not sig.**

Furthermore, when F–values of the model terms are compared, it can be observed that for all three response models, factor 1, corresponding to IRP, has a higher value and occurs more frequently than factor 2, ISC. This suggests that IRP has a greater effect on the responses than ISC. This is further supported by the perturbation plots shown in Figure 9, where a curvature signifies overall sensitivity of a response to a factor when the other is held constant. Since the line corresponding to factor 1 is more curved relative to the line corresponding to factor 2, the effects of IRP are relatively greater than the effects of ISC.

4.2.2 Summary of model equations and fit statistics

Table 9 provides the estimated coefficients, both coded and actual, and standard errors for constructing the model equations. The coded estimates are established based on the coded lows and highs (±1 levels) and can be used for comparison of the relative effects of the predictor terms on the response. For instance, the coded numerical coefficients associated with factor 1, IRP, have absolute values greater than those of factor 2, ISC. This meant that reactor pH is generally a better predictor and thus, has a greater effect on the responses as opposed to the concentration of substrate available for the microorganisms in the reactors [19], [46].

Factor interactions are also numerically described with predictor terms that contain both F1 and F2 to varying degrees. Albeit it would be difficult to completely understand its physical implications, these terms are necessary for the models' accuracy analytically, which is characteristic of empirical models.

4.2.2 Summary of model equations and fit statistics

Table 9 provides the estimated coefficients, both coded and actual, and standard errors for constructing the model equations. The coded estimates are established based on the coded lows and highs (±1 levels) and can be used for comparison of the relative effects of the predictor terms on the response.

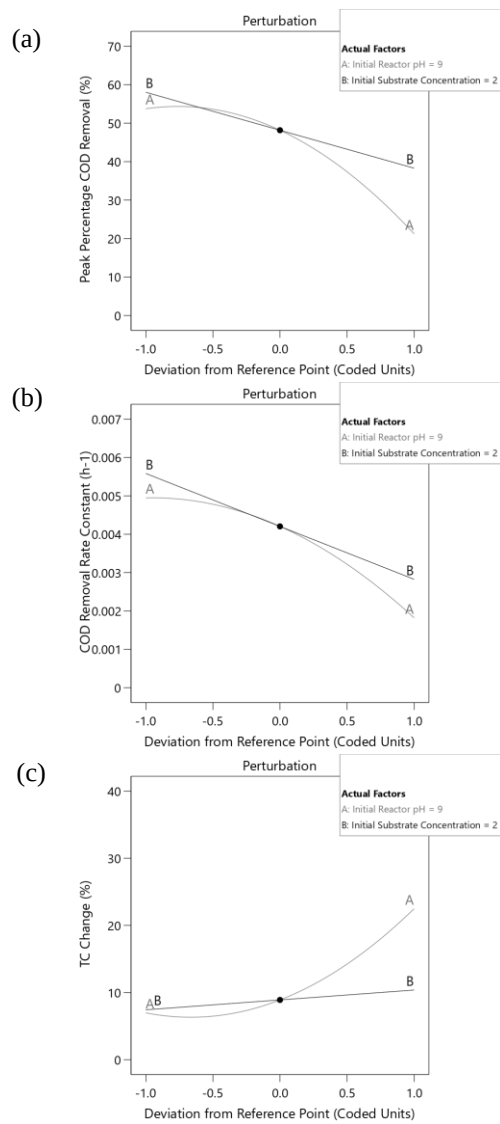

Figure 9: Perturbation plots for COD removal (a), COD removal rate constant (b), and TC change (c).

For instance, the coded numerical coefficients associated with factor 1, IRP, have absolute values greater than those of factor 2, ISC. This meant that reactor pH is generally a better predictor and thus, has a greater effect on the responses as opposed to the concentration of substrate available for the microorganisms in the reactors [19], [46].

Factor interactions are also numerically described with predictor terms that contain both F1 and F2 to varying degrees. Albeit it would be difficult to completely understand its physical implications, these terms are necessary for the models' accuracy analytically, which is characteristic of empirical models.

Table 9: Model equations coefficient estimates.

Predictor Term	Coefficient Estimate (Coded)	Standard Error	Coefficient Estimate (Actual)
Peak Percentage COD Removal (Reduced Cubic)			
Intercept	+48.16	1.57	-408.91224
F1	-16.25	1.53	+111.03287
F2	-9.86	2.17	+157.03469
F1F2	-3.05	2.17	-35.56363
$F1^2$	-10.67	1.63	-6.45055
$F1^2F2$	+7.56	3.07	+1.89103
COD Removal Rate Constant (Reduced Cubic)			
Intercept	+0.0042	0.0002	-0.073069
F1	-0.0016	0.0002	+0.018066
F2	-0.0014	0.0002	+0.033856
F1F2	-0.0005	0.0002	-0.007580
$F1^2$	-0.0008	0.0002	-0.001019
$F1^2F2$	+0.0016	0.0003	+0.000407
True Color Change (Reduced Quadratic)			
Intercept	+8.90	1.06	+104.43057
F1	+7.75	1.03	-24.05972
F2	+1.47	1.03	-6.17751
F1F2	+1.70	1.46	+0.850000
$F1^2$	+5.83	1.10	+1.45761

On the other hand, the actual estimates are based on the actual units of the factors: 7.00 – 11.0 for IRP and 1 %v/v – 3 %v/v for ISC. Although comparison can still be done indirectly, these coefficients are particularly useful if the responses are to be calculated using actual measurements of factors as inputs, eliminating the need for conversion into coded values. Table 10 is the summary of fit statistics for the models established for the three responses. Reduced cubic models were used to model the first two responses while a reduced quadratic model was used the third response.

Table 10: Summary of fit statistics for improved analysis.

Peak Percentage COD Removal (Reduced Cubic)			
Standard Deviation	4.34	RSQ	0.962
Mean	41.59	Adjusted RSQ	0.936
Coefficient of Variation %	10.43	Predicted RSQ	0.777
		Adequate Precision	19.779
COD Removal Rate Constant (Reduced Cubic)			
Standard Deviation	0.0004	RSQ	0.962
Mean	0.0037	Adjusted RSQ	0.936
Coefficient of Variation %	11.57	Predicted RSQ	0.827
		Adequate Precision	19.937
TC Change (Reduced Quadratic)			
Standard Deviation	2.92	RSQ	0.917
Mean	12.49	Adjusted RSQ	0.875
Coefficient of Variation %	23.41	Predicted RSQ	0.796
		Adequate Precision	13.663

High values of RSQ were observed for all three models: 0.9624, 0.9627, and 0.9165, respectively. Additionally, high values of adjusted RSQ, 0.9355, 0.9361, and 0.8747, respectively, ensured that predictor terms in the model contribute significantly to the model. Since the predicted RSQ values – 0.7770, 0.8269, and 0.7961, respectively – also reasonably agree with the values of the adjusted RSQ, this means that the models are not overfitted to the actual data.

Furthermore, the shown lack of overfitting and low values of the coefficient of variation –10.43%, 11.57%, and 23.41% – suggest replicability of results. Lastly, the obtained adequate precision values are all greater than 4.0, which means that there is a strong signal–to–noise ratio, implying that all three models can be used to navigate the design space while ensuring a precise result.

To further strengthen the models' reliability, outlier identification using plots of externally studentized residuals is analyzed. Studentized residuals are standardized deleted residuals, which are obtained by getting the difference between an excluded observation and the regression model from which it is excluded. By standardization, we can directly compare it to a normal plot from which we draw our interpretations. For all three responses, the plots of residuals lie close to the normal line as shown in Figure 10(a), (c), and (e). Since all values lie within the threshold set for externally studentized residuals in the plots of residuals against runs in Figure 10(b), (d), and (f), it can be said that there are no outliers that

influence the models' quality. This means that there is no single data point that influences the model more than the others and all data points are equally valid in creating the model.

Three–dimensional surface and contour plots for the models are provided in Figure 11 where the gray areas near the center are the maximal regions for each of the response variables. These plots visually show the interactive effects between the two factors, IRP and ISC, on the responses as predicted by the model equations.

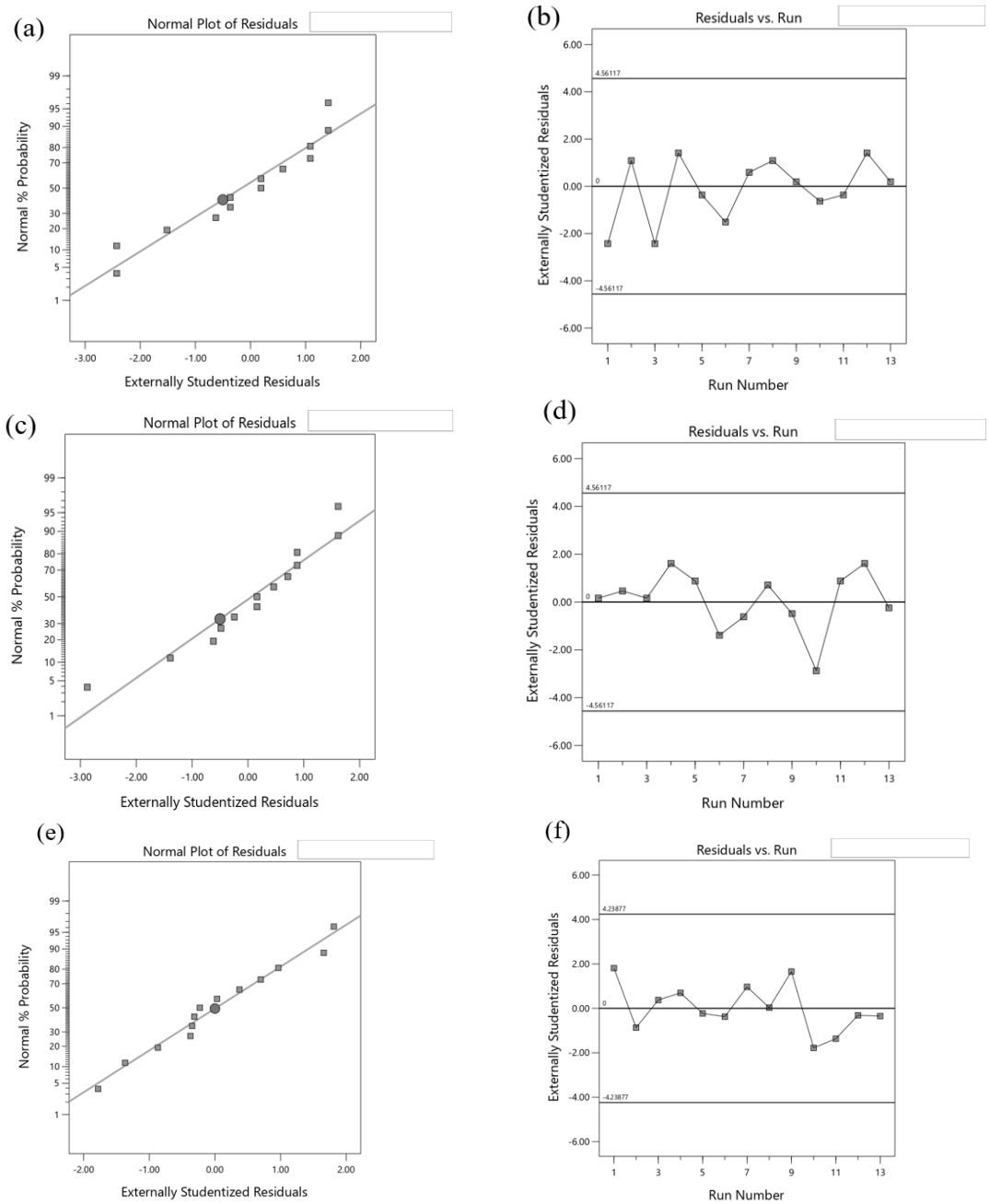

Figure 10: Externally studentized residuals plotted against a normal probability line and run values for COD removal (a, b), COD removal rate constant (c, d), and TC change (e, f).

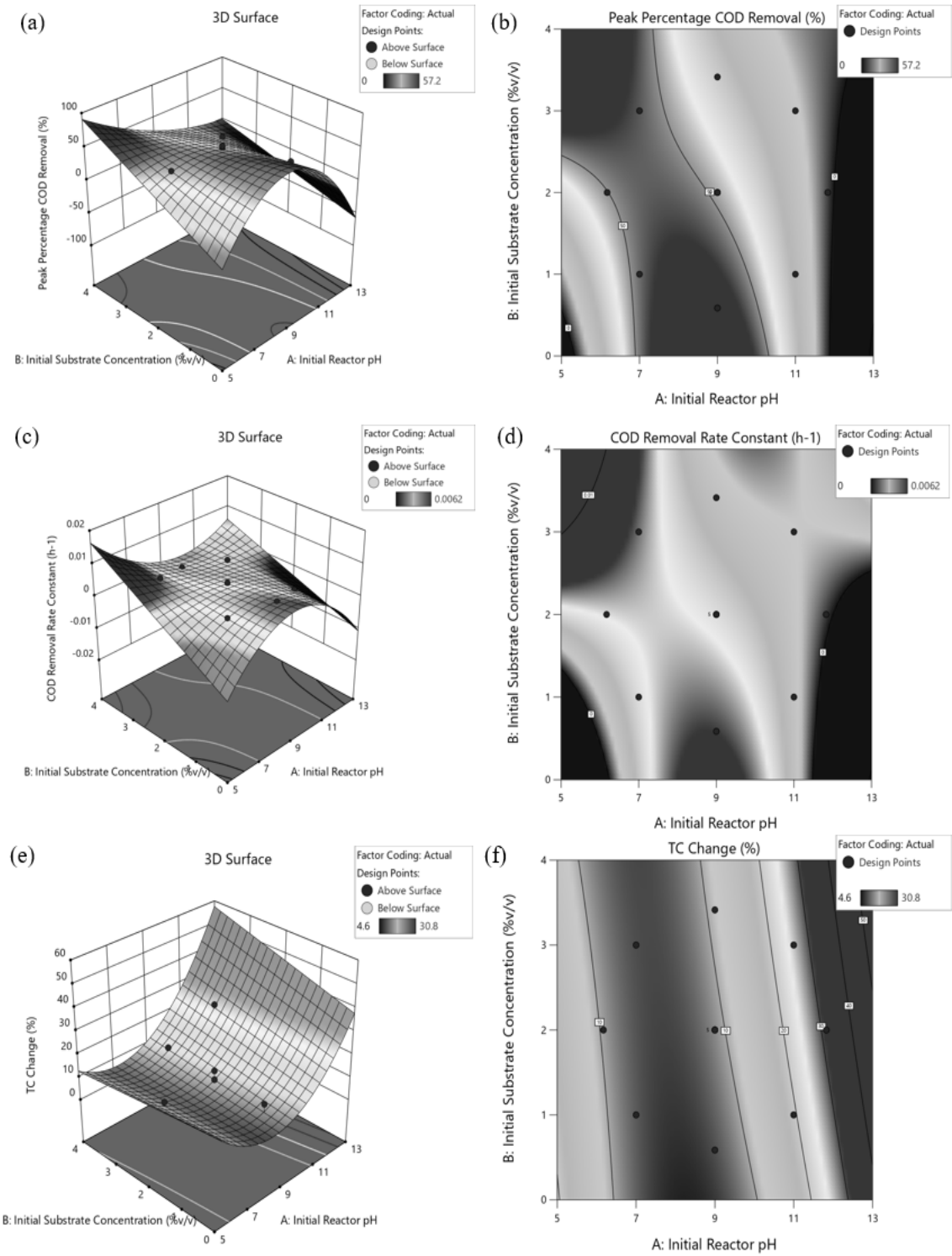

Figure 11: Three–dimensional surface and contour plots for peak percentage COD removal (a, b), COD removal rate constant (c, d), and TC change (e, f).

4.3 *Optimization*

To optimize the three response variables, both the IRP and ISC factors were set to be in the same range as the design space. The requirement set for optimization is for both the IRP and ISC to remain within the range. Individual maximizing optimizations were done initially, then three–response maximizing optimization was done with the same weights applied to the responses. Three representative solutions for each optimization are shown in Table 11.

It can be observed that when optimizing a single response only, the desirability values of the top solutions are in the range of 0.804 to 1.000. However, when all three responses are maximized simultaneously with the same weights, the desirability of the top solution is only 0.548.

Table 11: Sample initial optimization solutions.

F1	F2	R1	R2	R3	Desirability
Optimization of Peak Percentage COD Removal					
8.569	1.038	59.686	0.006	6.440	1.000
7.500	1.100	57.337	0.005	6.190	1.000
8.300	1.163	59.133	0.005	6.170	1.000
Optimization of COD Removal Rate Constant					
8.566	1.000	60.031	0.006	6.393	0.919
7.000	3.000	54.491	0.006	6.753	0.919
8.528	1.000	60.126	0.006	6.327	0.919
Optimization of TC Change					
11.000	3.000	15.883	0.002	25.662	0.804
10.958	3.000	16.411	0.002	25.226	0.787
11.000	2.846	16.707	0.002	25.173	0.785
Optimization of All Three Responses					
10.078	1.000	45.601	0.004	12.392	0.548
10.057	1.000	45.946	0.004	12.262	0.548
10.102	1.000	45.217	0.004	12.536	0.548

One reason is that high TC change values occur at higher IRP levels, as observed previously in the TC change data. This contrasts with both the COD removal rate effectiveness and the COD removal rate constant, whose high values occur at lower IRP levels. And since IRP is a significant factor among these three responses, this means that using low or high levels of IRP will come at the cost of desirability either way.

Monitoring the pH of the reactors, however, revealed that all 13 reactors approached a pH within the range of 8.30 – 9.29 (Figure 12). As this is potentially the steady-state pH of operating the reactors, the optimization range for IRP was set to be equivalent to these values.

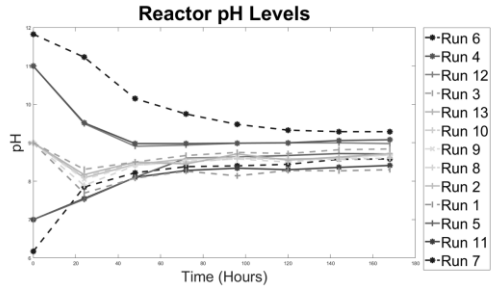

Figure 12: Reactor pH levels through time.

These results are further supported by the rate constant plots, peaking in the same region of pH, as previously observed. Also, since it is ideally better to have a high influent for wastewater treatment, the goal for the ISC was set to maximize optimization, albeit the rate constant plots also peak in the low ISC region.

Table 12 shows the list of possible solutions when the responses are still set to be maximized individually and at equal importance and the factors are constrained. When all three responses are maximized simultaneously with the same weights of importance, the desirability of the top solution is only 0.516, which still underscores the necessity of separate treatment stages.

Table 12: Constrained optimization solutions.

F1	F2	R1	R2	R3	Desirability
Optimization of Peak Percentage COD Removal					
8.300	3.000	44.672	0.004	7.782	0.884
8.300	2.979	44.835	0.004	7.764	0.881
8.300	2.967	44.933	0.004	7.753	0.879
Optimization of COD Removal Rate Constant					
8.300	3.000	44.672	0.004	7.782	0.767
8.300	2.970	44.910	0.004	7.755	0.764
8.375	3.000	44.024	0.004	7.992	0.757
Optimization of TC Change					
9.290	3.000	35.432	0.003	11.870	0.527
9.203	3.000	36.303	0.003	11.398	0.509
9.078	3.000	37.543	0.003	10.752	0.485
Optimization of All Three Responses					
9.290	2.846	36.994	0.003	11.606	0.516
9.290	2.837	37.087	0.003	11.590	0.516
9.290	2.860	36.849	0.003	11.630	0.516

To further check the models' validity, five additional runs were conducted using one of the solutions proposed for optimizing R1. The obtained results were compared to the models' predictions. The mean peak percentage COD removal of 43.2%, mean COD removal rate constant of 0.0037, and mean TC

change of 7.0 are well within the 95% confidence interval of the predicted values: 44.67%, 0.0036, and 7.8%, respectively.

5 Conclusions

In summary, results revealed that optimization of one response variable at a time provides optimal solutions with high desirability values. Prior to adjustments, sample optimal conditions for peak percentage COD removal include an IRP of 8.569 and an ISC of 1.038 %v/v. Meanwhile, optimal conditions for the COD reactor rate constant include an IRP of 8.566 and an ISC of 1.000 %v/v. For percentage TC change, optimal conditions include an IRP of 11.000 and an ISC of 3.000 %v/v. However, optimization of all three variables at once produced solutions with desirability values around 0.548. It was shown that maximizing TC change contradicts the maximization of the first two responses in terms of pH levels. With these, it can be argued that treatment should be done in separate stages, one that maximizes COD removal and removal rate, and the other geared towards color and turbidity parameters. This also eliminates the necessity for optimization for reaction time. The significance of the obtained models and their implications suggest the effectiveness of using RSM-CCD in navigating the design space for the variables and providing insights into the treatment process. Additionally, this work also utilized a kinetic modelling approach to model COD removal rates. It was found that a pseudo-first order kinetics best represent the reactors in the design space with an average RSQ value of 0.8556. Sigmoidal models also produced high RSQ values of over 0.83, which shows possibilities of application in similar systems.

Acknowledgments

This study is based on the preliminary works of S.C. Wu and his team on the alkaliphilic bacterial consortium they are using to treat PGME-AWD. The contents of this thesis are completely original works by the author, L.A. Rovillos, and were written under the constant guidance of K.G. Quiton, K.R. Pamintuan, and S.C. Wu and the support of Mapúa University and National Chung Hsing University.

Author Contributions

L.A.: conceptualization, methodology, software, validation, analysis, investigation, data curation, original draft preparation, reviewing and editing, visualization; K.G.: conceptualization, software, validation, analysis, review, supervision; K.R.: validation, analysis, resources, review, supervision; S.C.: conceptualization, validation, analysis, resources, review, supervision, project administration and economy. All authors have read and agreed to the published version of the manuscript.

Conflicts of Interest

The authors declare no conflict of interest.

Declaration of generative AI and AI-assisted technologies in the writing process

The authors utilized the ChatGPT and Google NotebookLM tools only to assist in enhancing the language and readability of the manuscript.

References

[1] H. D. Doan, A. Weli, and J. Wu, "A combined photocatalytic and electrochemical treatment of wastewater containing propylene glycol methyl ether and metal ions," *Chemical Engineering Journal*, vol. 151, no. 1–3, pp. 51–58, Aug. 2009, doi: 10.1016/j.cej.2009.01.041.

[2] Y. Huang et al., "Chemical characterization and source attribution of organic pollutants in industrial wastewaters from a Chinese chemical industrial park," *Environmental Research*, vol. 229, Jul. 2023, Art. no. 115980, doi: 10.1016/j.envres.2023.115980.

[3] S. Sandhu, A. Zumeit, Z. Tian, V. Vinciguerra, and R. Dahiya, "Semiconductor manufacturing wastewater challenges and the potential solutions via printed electronics," *iScience*, vol. 28, no. 10, Oct. 2025, Art. no. 113576, doi: 10.1016/j.isci.2025.113576.

[4] J. Sim et al., "A review of semiconductor wastewater treatment processes: Current status, challenges, and future trends," *Journal of Cleaner Production*, vol. 429, Dec. 2023, Art. no. 139570, doi: 10.1016/j.jclepro.2023.139570.

[5] J. LaDou, "Printed circuit board industry," *International Journal of Hygiene and Environmental Health*, vol. 209, no. 3, pp. 211–219, May 2006, doi: 10.1016/j.ijheh.2006.02.001.

[6] R. E. Parker and N. S. Isaacs, "Mechanisms of epoxide reactions," *Chemical Reviews*, vol. 59, no. 4, pp. 737–799, Aug. 1959, doi: 10.1021/cr50028a006.

[7] S. Liang, Y. Zhou, H. Liu, T. Jiang, and B. Han, "Synthesis of propylene glycol methyl ether catalyzed by MCM-41," *Synthetic Communications*, vol. 41, no. 6, pp. 891–897, Feb. 2011, doi: 10.1080/00397911003707089.

[8] World Semiconductor Trade Statistics. "WSTS semiconductor market forecast fall 2023." wsts.org. Accessed: Feb. 13, 2024. [Online.] Available: https://www.wsts.org/76/103/WSTS-Semiconductor-Market-Forecast-Fall-2023

[9] S. S. Chan, K. S. Khoo, K. W. Chew, T. C. Ling, and P. L. Show, "Recent advances biodegradation and biosorption of organic compounds from wastewater: Microalgae-bacteria consortium - A review," *Bioresource Technology*, vol. 344, Jan. 2022, Art. no. 126159, doi: 10.1016/j.biortech.2021.126159.

[10] V. Nagabalaji, P. Maharaja, R. Nishanthi, G. Sathish, R. Suthanthararajan, and S. V. Srinivasan, "Effect of co-culturing bacteria and microalgae and influence of inoculum ratio during the biological treatment of tannery wastewater," *Journal of Environmental Management*, vol. 341, Sep. 2023, Art. no. 118008, doi: 10.1016/j.jenvman.2023.118008.

[11] Y. Zhao et al., "Insights into biofilm carriers for biological wastewater treatment processes: Current state-of-the-art, challenges, and opportunities," *Bioresource Technology*, vol. 288, Sep. 2019, Art. no. 121619, doi: 10.1016/j.biortech.2019.121619.

[12] R. Sathya, M. V. Arasu, N. A. Al-Dhabi, P. Vijayaraghavan, S. Ilavenil, and T. S. Rejiniemon, "Towards sustainable wastewater treatment by biological methods – A challenges and advantages of recent technologies," *Urban Climate*, vol. 47, Jan. 2023, Art. no. 101378, doi: 10.1016/j.uclim.2022.101378.

[13] W. Shi, Q. Li, R. Qi, H. Tang, and B. Zhang, "Fe3S4/persulfate-based pre-oxidation for mitigating membrane fouling and enhancing synergistic perfluorooctanoic acid removal: Influence of pH and persulfate types," *Journal of Membrane Science*, vol. 692, Feb. 2024, Art. no. 122316, doi: 10.1016/j.memsci.2023.122316.

[14] N. C. Lu and J. C. Liu, "Removal of phosphate and fluoride from wastewater by a hybrid precipitation–microfiltration process," *Separation and Purification Technology*, vol. 74, no. 3, pp. 329–335, Sep. 2010, doi: 10.1016/j.seppur.2010.06.023.

[15] P. P. Kanekar, S. S. Nilegaonkar, S. S. Sarnaik, and A. S. Kelkar, "Optimization of protease activity of alkaliphilic bacteria isolated from an alkaline lake in India," *Bioresource Technology*, vol. 85, no. 1, pp. 87–93, Oct. 2002, doi: 10.1016/S0960-8524(02)00018-4.

[16] United Nations General Assembly. "Transforming our world: The 2030 agenda for sustainable development." sdgs.un.org. Accessed: Mar. 26, 2025. [Online.] Available: https://sdgs.un.org/publications/transforming-our-world-2030-agenda-sustainable-development-17981

[17] N. Iberache et al., "Removal of the insecticide imidacloprid from water in commercial formulation using electro-Fenton and photo-electro-Fenton: Optimization of COD removal through response surface methodology RSM-CCD," *Chemical Engineering and Processing - Process Intensification*, vol. 196, Feb. 2024, Art. no. 109633, doi: 10.1016/j.cep.2023.109633.

[18] C. F. Bustillo-Lecompte and M. Mehrvar, "Treatment of an actual slaughterhouse wastewater by integration of biological and advanced oxidation processes: Modeling, optimization, and cost-effectiveness analysis," *Journal of Environmental Management*, vol. 182, pp. 651–666, Nov. 2016, doi: 10.1016/j.jenvman.2016.07.044.

[19] K. A. Kumar et al., "Optimization for removal of COD and BOD through RSM-CCD by activated sludge treatment process for pharmaceutical wastewater," *Journal of Environmental Nanotechnology*, vol. 12, no. 4, pp. 68–86, Dec. 2023, doi: 10.13074/jent.2023.12.234486.

[20] J. N. Neetha, K. Sandesh, K. Girish Kumar, B. Chidananda, and P. Ujwal, "Optimization of Direct Blue-14 dye degradation by Bacillus

fermus (Kx898362) an alkaliphilic plant endophyte and assessment of degraded metabolite toxicity," *Journal of Hazardous Materials*, vol. 364, pp. 742–751, Feb. 2019, doi: 10.1016/j.jhazmat.2018.10.074.

[21] I. Tiago, A. P. Chung, and A. Veríssimo, "Bacterial diversity in a nonsaline alkaline environment: Heterotrophic aerobic populations," *Applied and Environmental Microbiology*, vol. 70, no. 12, pp. 7378–7387, Dec. 2004, doi: 10.1128/AEM.70.12.7378-7387.2004.

[22] W. D. Grant, "Cultivation of aerobic alkaliphiles," *Methods in Microbiology*, vol. 35, pp. 439–449, 2006. doi: 10.1016/S0580-9517(08)70021-7.

[23] S. Tizazu, G. Tesfaye, B. Andualem, A. Wang, and A. Guadie, "Evaluating the potential of thermo-alkaliphilic microbial consortia for azo dye biodegradation under anaerobic-aerobic conditions: Optimization and microbial diversity analysis," *Journal of Environmental Management*, vol. 323, Dec. 2022, Art. no. 116235, doi: 10.1016/j.jenvman.2022.116235.

[24] I. M. E. Hassan, "Irregular boundary area computation by Simpson's 3/8 rule," *Journal of Surveying Engineering*, vol. 113, no. 3, pp. 127–132, Oct. 1987, doi: 10.1061/(ASCE)0733-9453(1987)113:3(127).

[25] B. Liengme and K. Hekman, "Numerical integration," in *Liengme's Guide to Excel® 2016 for Scientists and Engineers*, Amsterdam, Netherlands: Elsevier, 2020, pp. 317–336. doi: 10.1016/B978-0-12-818249-9.00013-3.

[26] G. Guo et al., "Decolorization and detoxification of azo dye by halo-alkaliphilic bacterial consortium: Systematic investigations of performance, pathway and metagenome," *Ecotoxicology and Environmental Safety*, vol. 204, Nov. 2020, Art. no. 111073, doi: 10.1016/j.ecoenv.2020.111073.

[27] R. G. Saratale, G. D. Saratale, D. C. Kalyani, J. S. Chang, and S. P. Govindwar, "Enhanced decolorization and biodegradation of textile azo dye Scarlet R by using developed microbial consortium-GR," *Bioresource Technology*, vol. 100, no. 9, pp. 2493–2500, May 2009, doi: 10.1016/j.biortech.2008.12.013.

[28] Z. Khan, K. Jain, A. Soni, and D. Madamwar, "Microaerophilic degradation of sulphonated azo dye – Reactive Red 195 by bacterial consortium AR1 through co-metabolism," *International Biodeterioration and Biodegradation*, vol. 94, pp. 167–175, Oct. 2014, doi: 10.1016/j.ibiod.2014.07.002.

[29] M. S. Khehra, H. S. Saini, D. K. Sharma, B. S. Chadha, and S. S. Chimni, "Decolorization of various azo dyes by bacterial consortium," *Dyes and Pigments*, vol. 67, no. 1, pp. 55–61, Oct. 2005, doi: 10.1016/j.dyepig.2004.10.008.

[30] A. A. Vaighan, M. R. A. Moghaddam, and S. H. Hashemi, "Effect of dye concentration on sequencing batch reactor performance," *Iranian Journal of Environmental Health Science and Engineering*, vol. 6, no. 1, pp. 11–16, Jan. 2009.

[31] Md. Z. Hossen, Md. E. Hussain, A. Hakim, K. Islam, Md. N. Uddin, and A. K. Azad, "Biodegradation of reactive textile dye Novacron Super Black G by free cells of newly isolated Alcaligenes faecalis AZ26 and Bacillus spp obtained from textile effluents," *Heliyon*, vol. 5, no. 7, Jul. 2019, Art. no. e02068, doi: 10.1016/j.heliyon.2019.e02068.

[32] A. Trivedi, S. Desireddy, and S. P. Chacko, "Effect of pH, salinity, dye, and biomass concentration on decolourization of Azo Dye Methyl Orange in denitrifying conditions," *Water*, vol. 14, no. 22, Nov. 2022, Art. no. 3747, doi: 10.3390/w14223747.

[33] M. Priyatharishini and N. M. Mokhtar, "Performance of jackfruit (Artocarpus heterophyllus) peel coagulant in turbidity reduction under different pH of wastewater," *Materials Today: Proceedings*, vol. 46, pp. 1818–1823, 2021, doi: 10.1016/j.matpr.2020.10.248.

[34] M. A. D. Flores Alarcón et al., "Efficient dye removal from real textile wastewater using orange seed powder as suitable bio-adsorbent and membrane technology," *Water*, vol. 14, no. 24, Dec. 2022, Art. no. 4104, doi: 10.3390/w14244104.

[35] J.-S. Chang, C. Chou, Y.-C. Lin, P.-J. Lin, J.-Y. Ho, and T. Lee Hu, "Kinetic characteristics of bacterial azo-dye decolorization by Pseudomonas luteola," *Water Research*, vol. 35, no. 12, pp. 2841–2850, Aug. 2001, doi: 10.1016/S0043-1354(00)00581-9.

[36] S. Ertuğrul, M. Bakır, and G. Dönmez, "Treatment of dye-rich wastewater by an immobilized thermophilic cyanobacterial strain: Phormidium sp.," *Ecological*

Engineering, vol. 32, no. 3, pp. 244–248, Mar. 2008, doi: 10.1016/j.ecoleng.2007.11.011.

[37] G. D. Saratale, R. G. Saratale, J. S. Chang, and S. P. Govindwar, "Fixed-bed decolorization of Reactive Blue 172 by Proteus vulgaris NCIM-2027 immobilized on Luffa cylindrica sponge," *International Biodeterioration and Biodegradation*, vol. 65, no. 3, pp. 494–503, Jun. 2011, doi: 10.1016/j.ibiod.2011.01.012.

[38] T. P. Thao, H.-C. Kao, R.-S. Juang, and J. C.-W. Lan, "Kinetic characteristics of biodegradation of methyl orange by Pseudomonas putida mt2 in suspended and immobilized cell systems," *Journal of the Taiwan Institute of Chemical Engineers*, vol. 44, no. 5, pp. 780–785, Sep. 2013, doi: 10.1016/j.jtice.2013.01.015.

[39] M. K. Hafshejani, C. J. Ogugbue, and N. Morad, "Application of response surface methodology for optimization of decolorization and mineralization of triazo dye Direct Blue 71 by Pseudomonas aeruginosa," *3 Biotech*, vol. 4, no. 6, pp. 605–619, Dec. 2014, doi: 10.1007/s13205-013-0192-7.

[40] K. M. Zin, M. I. Effendi Halmi, S. S. Abd Gani, U. H. Zaidan, A. W. Samsuri, and M. Y. Abd Shukor, "Microbial decolorization of triazo dye, Direct Blue 71: An optimization approach using response surface methodology (RSM) and artificial neural network (ANN)," *BioMed Research International*, vol. 2020, Feb. 2020, Art. no. 2734135, doi: 10.1155/2020/2734135.

[41] M. S. A. Amin, F. Stüber, J. Giralt, A. Fortuny, A. Fabregat, and J. Font, "Comparative anaerobic decolorization of azo dyes by carbon-based membrane bioreactor," *Water*, vol. 13, no. 8, Apr. 2021, Art. no. 1060, doi: 10.3390/w13081060.

[42] N. Daneshvar, A. R. Khataee, M. H. Rasoulifard, and M. Pourhassan, "Biodegradation of dye solution containing Malachite Green: Optimization of effective parameters using Taguchi method," *Journal of Hazardous Materials*, vol. 143, no. 1–2, pp. 214–219, May 2007, doi: 10.1016/j.jhazmat.2006.09.016.

[43] M. H. Zwietering, I. Jongenburger, F. M. Rombouts, and K. van 't Riet, "Modeling of the bacterial growth curve," *Applied and Environmental Microbiology*, vol. 56, no. 6, pp. 1875–1881, Jun. 1990, doi: 10.1128/aem.56.6.1875-1881.1990.

[44] C. Liang, N. de Jonge, P. N. Carvalho, J. L. Nielsen, and K. Bester, "Biodegradation kinetics of organic micropollutants and microbial community dynamics in a moving bed biofilm reactor," *Chemical Engineering Journal*, vol. 415, Jul. 2021, Art. no. 128963, doi: 10.1016/j.cej.2021.128963.

[45] C. Liang, P. N. Carvalho, and K. Bester, "Effects of substrate loading on co-metabolic transformation pathways and removal rates of pharmaceuticals in biofilm reactors," *Science of The Total Environment*, vol. 853, Dec. 2022, Art. no. 158607, doi: 10.1016/j.scitotenv.2022.158607.

[46] J. R. Ruparelia and H. K. Patel, "Harnessing the chromium reduction potential of Pseudomonas aeruginosa JRHM33: A comprehensive study on bioinformatics, phenotype microarray, and CCD-RSM optimization," *Heliyon*, vol. 10, no. 15, Aug. 2024, Art. no. e35650, doi: 10.1016/j.heliyon.2024.e35650.